文章编号： 1007-8827(2018)04-0333-08

一步法合成 N,S 共掺杂荧光碳量子点及其检测汞离子性能

魏居孟[1]， 刘碧桃[2]， 张 欣[3]， 宋常春[1]

(1. 安徽科技学院 化学与材料工程学院，安徽 凤阳 233100；
2. 重庆文理学院 材料与化学工程学院，重庆 402160；
3. 西安科技大学 理学院，陕西 西安 710054)

摘 要： 采用简单一步水热法合成了高荧光量产率(FLQY，12.6%)的 N,S 共掺杂碳量子点(N，S-CQDs)。该碳量子点具有小的粒径,无定型结构,独特的表面态和依赖于激发光的荧光特性。N 和 S 的共掺杂促进了 N，S-CQDs 和 Hg^{2+} 离子之间的电子传递和协调相互作用。结果表明,该 N,S 共掺杂碳量子点在湖水中检测 Hg^{2+} 离子展现出了较高的灵敏度和选择性。因此,该碳量子点作为荧光探针在环境监测中具有很好的应用前景。

关键词： 碳量子点；L-半胱氨酸；共掺杂；荧光；Hg^{2+} 离子检测

中图分类号： TQ127.1+1 **文献标识码：** A

基金项目：安徽科技学院引进人才项目基金(ZRC2014448)；安徽科技学院重点学科基金(AKZDXK2015A01)；环境材料与修复技术重庆市重点实验室开放课题基金(CEK1502).

通讯作者：宋常春. E-mail：lzu_alice@163.com

One-pot synthesis of N, S co-doped photoluminescent carbon quantum dots for Hg^{2+} ion detection

WEI Ju-meng[1], LIU Bi-tao[2], ZHANG Xin[3], SONG Chang-chun[1]

(1. *College of Chemistry and Materials Engineering, Anhui Science and Technology of University, Fengyang* 233100, *China*;
2. *College of Materials and Chemical Engineering, Chongqing University of Arts and Sciences, Chongqing* 402160, *China*;
3. *College of Science, Xi'an University of Science and Technology, Xi'an* 710054, *China*)

Abstract: N and S co-doped carbon quantum dots (N, S-CQDs) with a high fluorescence quantum yield (12.6%) were synthesized by a one-pot hydrothermal method. Results indicate that the N, S-CQDs have a small particle size and an amorphous structure, exhibiting unique surface states and excitation wavelength-independent fluorescent properties. Co-doping of N and S increases the electron-transfer rate and improves the coordination interaction between the N, S-CQDs and Hg^{2+} ions. The N, S-CQDs show a high sensitivity and selectivity in detecting Hg^{2+} ions even for a lake water sample. They are promising fluorescence probes for environmental monitoring.

Key words: Carbon quantum dots; L-cysteine; Co-doped; Photoluminescent; Hg^{2+} ions detection

Received date: 2018-04-02; *Revised date*: 2018-06-06

Foundation item: Talent Introduction Foundation of Anhui Science and Technology of University (ZRC2014448); Key Discipline Foundation of Anhui Science and Technology of University (AKZDXK2015A01); Open Foundation of Chongqing Key Laboratory of Environmental & Remediation Technologies (CEK1502).

Corresponding author: SONG Chang-chun. E-mail: lzu_alice@163.com

English edition available online ScienceDirect (http://www.sciencedirect.com/science/journal/18725805).

DOI: 10.1016/S1872-5805(18)60343-9

1 Introduction

Heavy-metal ions are greatly hazardous to human health and ecological environments[1-4]. During the past few decades, industrial and other anthropogenic processes have been constantly releasing heavy-metal ions into the environment. Among them, the Hg^{2+} ions are never away from our sight due to its extreme toxicity, wide distribution and high industrial value[5,6]. According to research data, approximate 940 tons of Hg^{2+} ions are released to lithosphere and hydrosphere each year, which is seriously harmful to human and other organisms due to the hydrologic cycle and accumulation[7]. Conventional analytical techniques for the determination of Hg^{2+} ions have been successfully developed such as chromatography, spectrofluorimetry, and atomic absorption spectrometry[5,8]. However, most of these methods are not con-

venient due to the requirement of expensive equipment and complicated sample pretreatment. Accordingly, the development of advanced analytical techniques for Hg^{2+} ion detection is highly desired.

Compared with conventional analytical techniques, the fluorescent probe method possess a series of merits such as high sensitivity, high selectivity, and easy operation[9-11]. As an outstanding fluorescence probe material, carbon quantum dots (CQDs) have attracted growing interest owing to their distinct advantages such as low cost, simple synthesis route, good biocompatibility, low cytotoxicity, high photo and chemical stability, no blinking fluorescence, and tunable excitation and emission spectra. Up to date, the CQDs have been developed for the detection of Hg^{2+}, Cu^{2+}, Cr^{4+}, Fe^{3+}, et al. by monitoring the changes of their fluorescence intensities[12-15]. Among them, the doped, especially co-doped CQDs with different heteroatoms such as nitrogen and sulfur introduced more active sites and improved the fluorescent quantum yield (FLQY), leading to outstanding sensing performance[16-20]. Therefore, the investigation on co-doped CQDs with peculiar properties for use as fluorescent probes have never been stopped. Wang et al. used citric acid and dithiooxamide to fabricate N, S-CQDs and investigated the Hg^{2+} ion detection properties[21]. Xu's group employed heparin sodium to obtain N, S-CQDs and studied the performance for Fe^{3+} detection[22]. Nevertheless, it is still a challenge to prepare N, S-CQDs with novel properties via a facile and effective route.

In this work, a facile and simple strategy is developed for the hydrothermal synthesis of N, S-CQDs by using L-cysteine as the single precursor. It is found that both N and S atoms are doped in the CQDs. As-prepared N, S-CQDs exhibit a small particle size, good fluorescence performance, relatively high quantum yield up to 12.6%, and have been successfully applied in Hg^{2+} ion detection.

2 Experimental

2.1 Chemicals and reagents

L-cysteine (L-cys) with a purity of 99% was purchased from Aladdin Ltd. (Shanghai, China). All the other chemicals were purchased from Aladdin Ltd. (Shanghai, China) and used as received without further purification. All solutions were prepared using Milli-Q deionized water (18.2 MΩ cm^{-1}, Millipore) as the solvent throughout the experiments.

2.2 Synthesis of the N, S-CQDs

The N, S-CQDs were prepared by hydrothermal treatment of L-cys. The typical experimental procedure is shown in Scheme 1. Typically, 1.0 g L-cys was dissolved in 30 mL deionized (DI) water under agitation at room temperature, and then the solution was transferred to a stainless steel autoclave with a 50 mL Teflon liner and heated at 180 ℃ for 12 h. After cooled to room temperature naturally, the resulting yellow aqueous solution was centrifuged at 12 000 rpm for 20 min to remove the non-fluorescent deposit. The resultant supernate containing fluorescent N, S-CQDs was dialyzed (MWCO: 3500) against DI water for two days to remove inorganic ions and molecules. Finally, a clear and transparent N, S-CQD solution without any precipitation was obtained. On exposure to UV light (365 nm), the obtained solution shows a bright blue color.

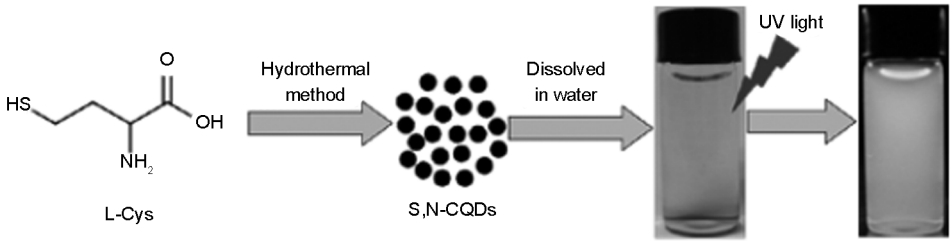

Scheme 1 Schematic of the preparation procedure of N, S-CQDs and the photograph of the N, S-CQDs solution excited by daylight and a 365 nm UV lamp.

2.3 Characterization

Transmission electron microscopy (TEM) images, high resolution TEM (HRTEM) images and selected area electron diffraction (SAED) were acquired by using a Tecnai-G^2 F30 transmission electron microscope operating at an acceleration voltage of 300 kV. X-Ray diffraction (XRD) measurements were performed on a Rigaku D/Max-2400 X-ray diffractometer using Cu $K\alpha$ radiation. The Fourier transform infrared (FTIR) spectra were measured by a Thermo Nicolet Nexus FTIR model 670 spectrometer. X-ray photoelectron spectroscopic (XPS) analysis was carried on an ESCALAB 250xi photoelectron spectrometer. UV-Vis spectroscopic studies were performed with a TU-1901 dual beam UV-Vis spectrophotometer. Photoluminescent (PL) measurements were carried out with a FLs920 steadystate/transientstate spectro xsort.

2.4 Metal ion detection

The obtained N, S-CQD solution was diluted 20 times to be the fluorescent probe. For the detection of various metal ions, $MnCl_2$, $CaCl_2$, $ZnCl_2$, $MgSO_4$, NaCl, $NiCl_2$, $AlCl_3$, $CdCl_2$, $CuCl_2$, $Pb(NO_3)_2$, $Hg(NO_3)_2$ were used as various ion sources. In a typical detection experiment, the solutions containing a calculated amount of ions were added into the N, S-CQDs solution. After mixing evenly, the PL spectra were detected at 365 nm excitation. All of the experiments were performed in phosphate buffer saline (PBS) unless stated otherwise.

3 Results and discussion

Fig. 1 represents a typical XRD profile of the N, S-CQDs. The (002) peak centers at 19.1° and the corresponding interlayer spacing is d = 0.425 nm, which is larger than that of graphite (0.34 nm)[23]. The increase in this value indicates an increase in amorphous nature, and is probably ascribed to the introduction of nitrogen-, sulfur- and oxygen-containing groups[24]. The poor crystalline nature of the N, S-CQDs is further confirmed by HRTEM image (in the set of Fig. 1b), from which no clear lattice fringes can be seen. Fig. 1b shows the TEM image of the N, S-CQDs, revealing that the N, S-CQDs have a spherical morphology and a narrow size distribution from 2.0 to 6.5 nm (inset of Fig. 1a).

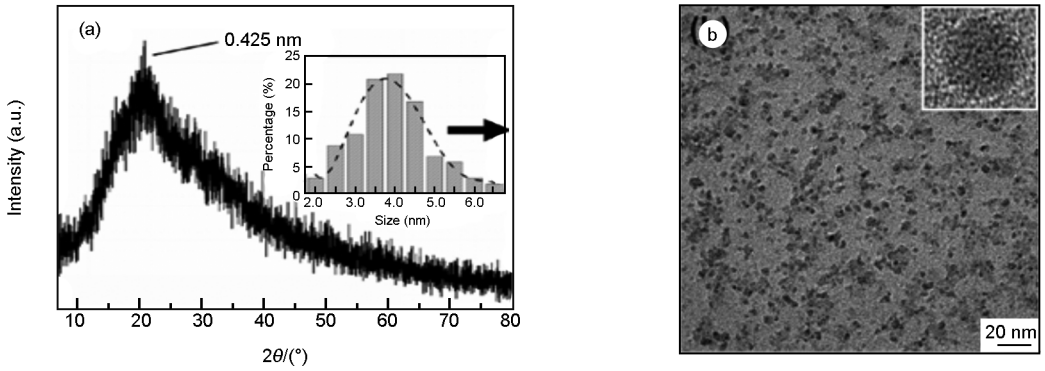

Fig. 1 (a) XRD pattern of the N, S-CQDs, inset: size distribution bar graph; (b) TEM image of the N, S-CQDs, inset: HRTEM image of one particle.

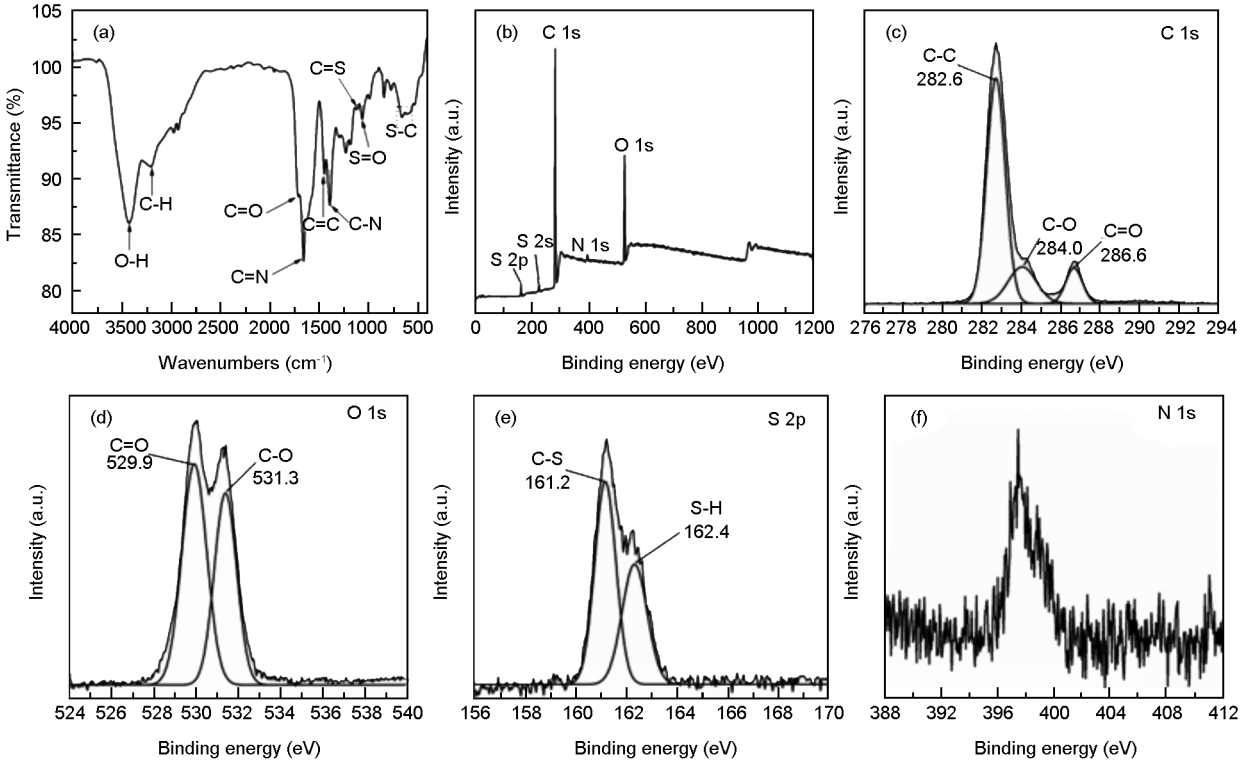

Fig. 2 Surface state and component characterization of N, S-CQDs: (a) FTIR spectrum; (b) XPS full scan spectrum; (c-f) high resolution scan XPS spectrum of C 1s, O 1s, S 2p and N 1s, respectively.

The surface functionalities were characterized by FTIR and XPS analysis. Fig. 2a represents the FTIR spectrum of the N, S-CQDs. The broad peak centered at about 3 429 cm^{-1} is attributed to the O—H and N—H stretching vibration, indicating the presence of hydroxyl and amino groups[25], which contributes to their favorable hydrophilicity. The band located at 3 205 cm^{-1} is caused by the C—H bonds, while the small peak observed at 1 715 cm^{-1} corresponds to C═O bonds[26]. The peaks at 1 658 and 1 450 cm^{-1} show the presence of C═N and C═C bonds, respectively[27]. The peaks at 1 394, 1 120 and 1 068 cm^{-1} can be identified as C—N, C═S and S═O bonds, respectively[25, 27]. Besides, there is a peak around 660 cm^{-1}, which is due to the C-S bonds[22, 27]. These bonds might be generated from the hydrothermal treatment of L-cys.

XPS was used to further investigate the elemental composition and surface chemical states of the N, S-CQDs. Fig. 2b shows the full scan XPS spectrum of the N, S-CQDs, and the five peaks at 161, 225, 283, 398 and 531 eV correspond to S 2p, S 2s, C 1s, N 1s and O 1s, respectively[28]. Besides, the full width at half maximum (FWHM) of S 2p, C 1s, N 1s and O 1s are 2.564, 2.373, 3.107 and 3.221 eV, and the content of C, O, N and S elements gathered by element analysis is 75.97, 17.73 (calculated by difference), 2.00 and 4.30 wt%, respectively. All these observations indicate that the carbon dots contain nitrogen, and sulfur elements. Deconvolution of the high resolution C 1s spectrum displays three peaks at 282.6, 284.0 and 286.6 eV corresponding to the C—C, C—O and C═O bonds, respectively[29]. The high-resolution O 1s spectrum of the N, S-CQDs shows two peaks (Fig. 2d) at 529.9 and 531.3 eV, which are attributed to the C═O and C—O bonds, respectively[30]. As shown in Fig. 2e, the high resolution S 2p XPS spectrum clearly shows two peaks at 161.2 and 162.4 eV, which represent S—C and S—H bonds, respectively[16,22]. Furthermore, the weak N signal has also been observed for the N, S-CQDs samples (Fig. 2f). All these experimental evidences are consistent with the FTIR results, demonstrating that the S and N elements were successfully co-doped into the carbon dots, which would give the CDs more outstanding properties.

Fig. 3a shows the UV-visible absorption spectrum of the N, S-CQDs with a characteristic absorption peak at 226 nm, which is ascribed to the π-π^* electronic transitions of C═C. A weak absorption peak around 318 nm is observed, which is corresponded to the n-π^* electronic transitions of C═N and C═O in the N, S-CQDs[31,32]. Under an excitation of 365 nm, the N, S-CQDs exhibit a strong emission at 438 nm, which corresponds to the blue fluorescence as shown in Fig. 1. Monitoring the emission at 425 nm produces a peak centered at 335 nm (Fig. 3b).

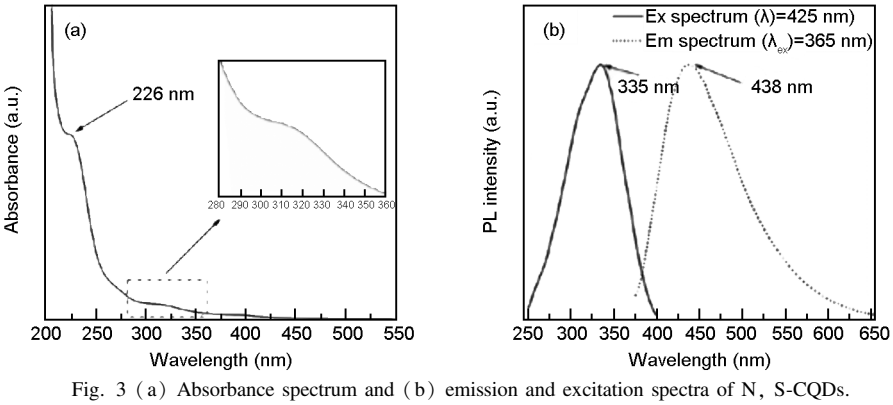

Fig. 3 (a) Absorbance spectrum and (b) emission and excitation spectra of N, S-CQDs.

The results of PL spectra of the N, S-CQDs (Fig. 4a) indicate that their emission wavelength is excitation-independent under the excitation wavelength ranges from 280 to 500 nm and the intensity of the emission peaks are relatively strong along with excitation wavelength ranging from 280 to 360 nm. Such excitation-dependent emission property has been reported as an important criterion for CQD materials. This is attributed to the inhomogenous carbogenic core emission in the sample, which results in the distribution of different emissive sites on each nanoparticles[33-35]. The PLQY of the CQDs was obtained by referencing to a standard (quinine sulphate in 0.1 M H_2SO_4) following the previous reports[36,37] according to the equation (1):

$$\varphi = \varphi' \left(\frac{m}{m'}\right) \left(\frac{\eta}{\eta'}\right)^2 \quad (1)$$

Where φ and φ' (54%) is the PLQY of sample and standard, m (sample, 3.61×10^9) and m' (standard, 1.546×10^{10}) is the slope with the plot of inte-

grated fluorescence intensity vs. absorbance, η (sample) and η' (standard) is the refractive index of the solvent (for the aqueous solutions $\eta/\eta' = 1$). The FLQY of the N, S-CQDs is calculated to be 12.6%, which is acceptable for their use as fluorescent probes. It is worth mentioning that reducing reaction temperature from 200 to 120 ℃ leads to a decrease in the PLQY from 13.9% to 8.4%. Fig. 4b shows the PL decay curve and the instrument response function, the observed lifetimes of the CQDs are $\tau_1 = 0.64$ ns, $\tau_2 = 3.05$ ns and $\tau_3 = 10.11$ ns, which reveals the radiative recombination nature of excitations. The calculated average lifetime is 4.25 ns. This lifetime located in the magnitude of nanosecond suggests that the N, S-CQDs are most suitable for optoelectronic applications[24,38].

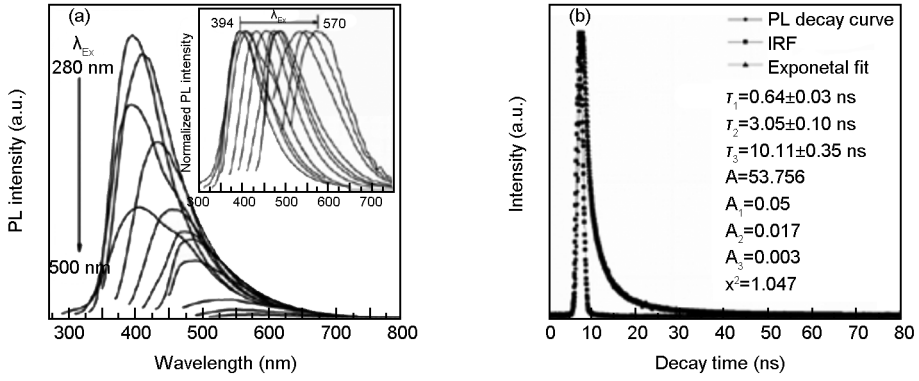

Fig. 4 PL emission spectra of N, S-CQDs with progressively longer excitation wavelengths from 280 to 500 nm, inset: normalized PL emission spectra; (b) PL decay curve of N, S-CQDs, inset: instrument response function.

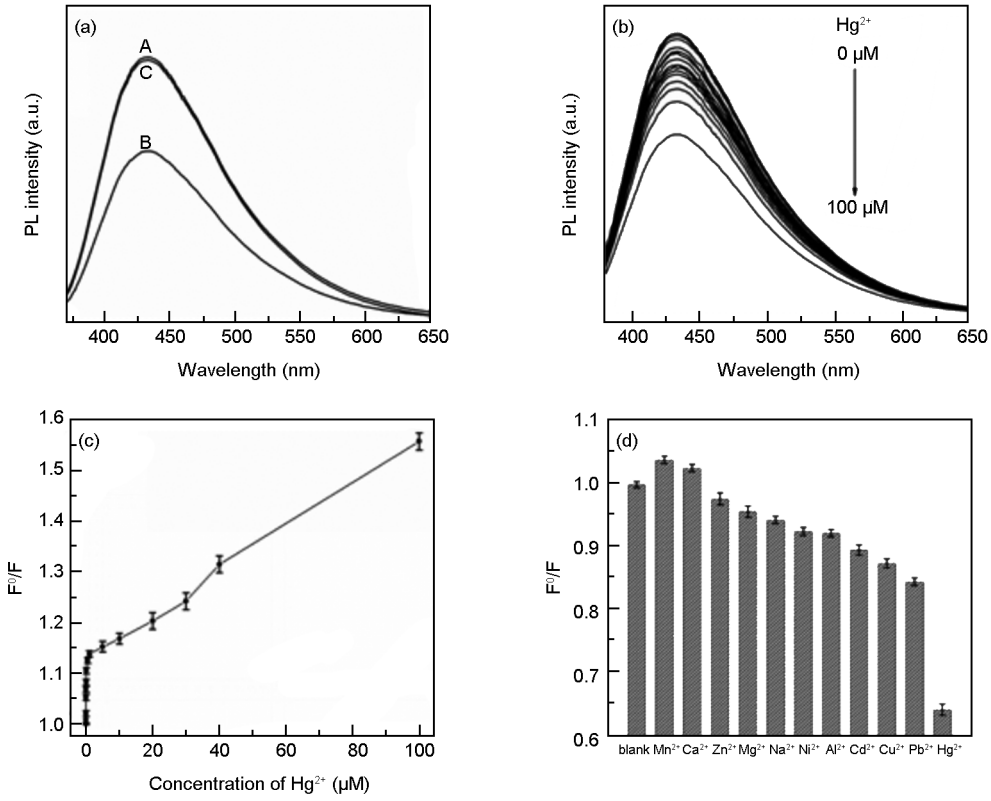

Fig. 5 (a) PL spectra of N, S-CQDs in the absence-(A), presence-(B) of Hg^{2+} ions and N, S-CQDs-Hg^{2+}-EDTA mixture-(C); (b) PL spectra of the CD dispersion in the presence of different Hg^{2+} ion concentrations(0, 0.001, 0.005, 0.01, 0.05, 0.1, 0.5, 1, 5, 10, 20, 30, 40, 50 and 100 μM); (c) the dependence of F^0/F on the concentrations of Hg^{2+} ions; (d) the dependence of F^0/F on the blank and solutions containing different metal ions (λ_{ex} = 360 nm, [ions] = 100 μM).

For qualitative detection of Hg^{2+} ions, as shown in Fig. 5a, the N, S-CQD solution in the absence of Hg^{2+} ions exhibits a strong PL peak at 433 nm (λ_{ex} = 360 nm). In contrast, the presence of Hg^{2+} ions leads to an obvious intensity decrease of fluorescence at the same test conditions, indicating that Hg^{2+} ions can effectively quench the fluorescence of the N, S-CQDs. This observation is attributed to the electron transfer from excited N, S-CQDs to Hg^{2+} ions, leading to substantial fluorescence quenching[39,40]. The possible quenching mechanism of the N, S-CQDs fluorescent probe is presented in Scheme 2. When ethylene diamine tetraacetic acid (EDTA) was employed as a strong Hg^{2+} ion chelator, the intensity of the PL emission peak was almost completely restored, which verifies the above theoretical explanation. In the following experiments, the selectivity of this detection system for Hg^{2+} ions was also carried out. Different concentrations of Hg^{2+} ions in the range of 0-100 μM (0, 0.001, 0.005, 0.01, 0.05, 0.1, 0.5, 1, 5, 10, 20, 30, 40, 50 and 100 μM) in the blank N, S-CQDs solution were tested. Fig. 4b shows the PL spectra of N, S-CQDs in the presence Hg^{2+} ionswith different concentrations, revealing that the PL intensity of the mixture is sensitive to Hg^{2+} concentration and decreases with the increase of Hg^{2+} concentration. The sensitivity limit can be as high as 1 nM, which is higher than those of traditional detection methods and is comparable to the previously reported works[18,40-42]. This accuracy exceed the maximum allowable Hg^{2+} level (10 nM) in drinking water as established by the Environmental Protection Agency (USA)[12]. To get insight into the fluorescence quenching mechanism involved, the fluorescence quenching data were analyzed by the Stern-Volmer equation (2),

$$\frac{F^0}{F} = 1 + K_{SV}[Q] \qquad (2)$$

where F^0 and F are the N, S-CQDs fluorescence intensities at 433 nm in the absence and presence of Hg^{2+} ions, respectively. $[Q]$ is the concentration of the quencher (i.e. Hg^{2+} ions), and K_{SV} is the Stern-Volmer constant. As shown in Fig. 5c, the Stern-Volmer plot does not fit a conventional linear Stern-Volmer equation, indicating both dynamic and static quenching processes occur in this sensing system[43-45].

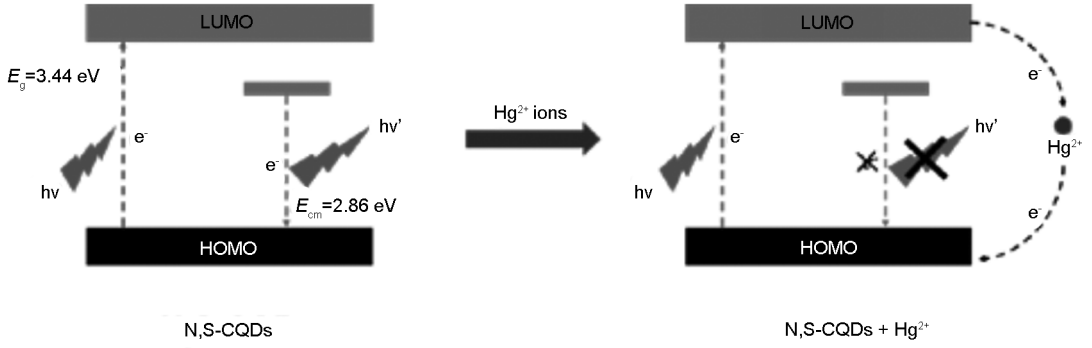

Scheme 2 The proposed FL quenching mechanism for N, S-CQDs system.

To evaluate the selectivity of the proposed Hg^{2+} sensor, the detection of Hg^{2+} was carried out in the presence of various representative metal ions under identical conditions with the same concentration of 100 μM. As shown in Fig. 5d, a much low PL intensity can be observed for the N, S-CQDs due to the addition of Hg^{2+}, while no obvious decrease is seen after adding other metal ions into the N, S-CQDs solution. The results reveal that the N, S-CQDs possess excellent ion selectivity, and the other metal ions have an ignorable interference on the sensing system. The high selectivity is probably assigned to the high affinity between Hg^{2+} and the functional groups on the surface of the N, S-CQDs.

As shown in Fig. 6a, an anti-interference Cd^{2+}, Cu^{2+}, or Pb^{2+} ions only have a slight influence on the fluorescence of the detection system. Furthermore, we also performed Hg^{2+} detection to evaluate this sensor in real water system, the analysis was challenged by lake water samples obtained from the local Longzi Lake of Bengbu, Anhui province, China. The lake water was centrifuged at 12 000 rpm for 20 min and filtered through membrane to remove the solid impurities and impurity inorganic ions. Subsequently, the Hg^{2+} ions with different concentrations were added into the resultant water samples and then analyzed with the proposed method. It is seen that the PL intensity decreases with increasing the concentration of Hg^{2+} ions from 0.5 to 20 μM (Fig. 6b), and the sensitivity limit is about 500 nM in spite of the interference from numerous minerals and organics existing in the lake water . These results imply the practical

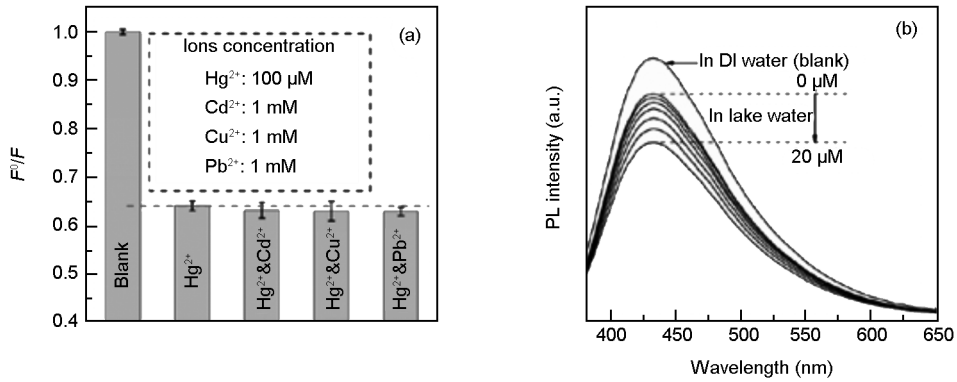

Fig. 6 (a) The dependence of F^0/F on the blank solutions, and the solutions containing Hg^{2+} ions and different interfering ions (λ_{ex} = 360 nm, [Hg^{2+}] = 100 μM, [Cd^{2+}] = [Cu^{2+}] = [Pb^{2+}] = 1 mM); (b) PL spectra of N, S-CQD dispersion in the presence of different Hg^{2+} concentrations (from top to bottom: 0, 0.5, 1, 2, 5, 10 and 20 μM) in lake water.

applicability for Hg^{2+} ion detection in environment monitoring.

4 Conclusion

One-pot hydrothermal treatment of L-cys has been performed for preparing N, S co-doped CQDs. The N, S-CQDs with a small size and higher FLQY have been further used as an outstanding sensing platform for detection of Hg^{2+} ions in DI water and a real water sample. This fluorescent probe with a fairly high sensitivity and selectivity provides a simple and fast route for sensing heavy-metal ions.

References

[1] Yang X, Wang E. A nanoparticle autocatalytic sensor for Ag^+ and Cu^{2+} ions in aqueous solution with high sensitivity and selectivity and its application in test paper[J]. Analytical Chemistry, 2011, 83(12): 5005-5011.

[2] Zhitkovich A. Chromium in drinking water: Sources, metabolism, and cancer risks[J]. Chemical Research in Toxicology, 2011, 24(10): 1617-1629.

[3] Yang Y, Jing L, Yu X, et al. Coating aqueous quantum dots with silica via reverse microemulsion method: Toward size-controllable and robust fluorescent nanoparticles[J]. Chemistry of Materials, 2007, 19(17): 4123-4128.

[4] Bera K, Das A K, Nag M, et al. Development of a rhodamine-rhodanine-based fluorescent mercury sensor and its use to monitor real-time uptake and distribution of inorganic mercury in live zebrafish larvae[J]. Analytical Chemistry, 2014, 86(5): 2740-2746.

[5] Nolan E M, Lippard S J. Tools and tactics for the optical detection of mercuric ion[J]. Chemical Reviews, 2008, 108(9): 3443-3480.

[6] Baughman T A. Elemental mercury spills[J]. Environ Health Perspect, 2006, 114(2): 147-152.

[7] Kim H N, Ren W X, Kim J S, et al. Fluorescent and colorimetric sensors for detection of lead, cadmium, and mercury ions [J]. Chemical Society Reviews, 2012, 41(8): 3210-3244.

[8] Aragay G, Pons J. A. Merkoci, recent trends in macro-, micro-, and nanomaterial-based tools and strategies for heavy-metal detection[J]. Chemical Reviews, 2011, 111(5): 3433-3458.

[9] YangY-K, Yook K-J, Tae J. A Rhodamine-based fluorescent and colorimetric chemodosimeter for the rapid detection of Hg^{2+} ions in aqueous media[J]. Journal of the American Chemical Society, 2005, 127(48): 16760-16761.

[10] Ngu P Z Z, Chia S P P, Fong J F Y, et al. Synthesis of carbon nanoparticles from waste rice husk used for the optical sensing of metal ions[J]. New Carbon Materials, 2016, 31(2): 135-143.

[11] Wang C, Zhang D, Huang X, et al. A ratiometric fluorescent chemosensor for Hg^{2+} based on FRET and its application in living cells[J]. Sensors and Actuators B: Chemical, 2014, 198(3): 33-40.

[12] Mohapatra S, Sahu S, Sinha N, et al. Synthesis of a carbon-dot-based photoluminescent probe for selective and ultrasensitive detection of Hg^{2+} in water and living cells[J]. Analyst, 2015, 140(4): 1221-1228.

[13] Wei J, Zhang X, Sheng Y, et al. Dual functional carbon dots derived from cornflour via a simple one-pot hydrothermal route [J]. Materials Letters, 2014, 123(10): 107-111.

[14] Zheng M, Xie Z, Qu D, et al. On-off-on fluorescent carbon dot nanosensor for recognition of chromium(VI) and ascorbic acid based on the inner filter effect[J]. ACS Applied Materials & Interfaces, 2013, 5(24): 13242-13247.

[15] Xu Q, Pu P, Zhao J, et al. Preparation of highly photoluminescent sulfur-doped carbon dots for Fe(III) detection[J]. Journal of Materials Chemistry A, 2015, 3(2): 542-546.

[16] Xue M, Zhang L, Zou M, et al. Nitrogen and sulfur co-doped carbon dots: A facile and green fluorescence probe for free chlorine[J]. Sensors and Actuators B: Chemical, 2015, 219: 50-56.

[17] Xu Q, Liu Y, Gao C, et al. Synthesis, mechanistic investigation, and application of photoluminescent sulfur and nitrogen co-doped carbon dots[J]. Journal of Materials Chemistry C, 2015, 3(38): 9885-9893.

[18] Hu C, Yu C, Li M, Wang X, et al. Chemically tailoring coal to fluorescent carbon dots with tuned size and their capacity for Cu(II) eetection[J]. Small, 2014, 10(23): 4926-4933.

[19] Li M, Hu C, Yu C, et al. Organic amine-grafted carbon quan-

tum dots with tailored surface and enhanced photoluminescence properties[J]. Carbon, 2015, 91: 291-297.
[20] Hu C, Yu C, Li M, et al. Nitrogen-doped carbon dots decorated on graphene: a novel all-carbon hybrid electrocatalyst for enhanced oxygen reduction reaction[J]. Chemical Communications, 2015, 51: 3419-3422.
[21] Wang Y, Kim S H, Feng L. Highly luminescent N, S- Co-doped carbon dots and their direct use as mercury(II) sensor [J]. Analytica Chimica Acta, 2015, 890: 134-142.
[22] Sun Y, Shen C, Wang J, et al. Facile synthesis of biocompatible N, S-doped carbon dots for cell imaging and ion detecting [J]. RSC Advances, 2015, 5(21): 16368-6375.
[23] De B and Karak N. A green and facile approach for the synthesis of water soluble fluorescent carbon dots from banana juice [J]. RSC Advances, 2013, 3(22): 8286-8290.
[24] Peng J, Gao W, Gupta B K, et al. Graphene quantum dots derived from carbon fibers[J]. Nano Letters, 2012, 12(2): 844-849.
[25] Zeng Y W, Ma D K, Wang W, et al. N, S co-doped carbon dots with orange luminescence synthesized through polymerization and carbonization reaction of amino acids[J]. Applied Surface Science, 2015, 342: 136-143.
[26] Liu J, Liu X, Luo H, et al. One-step preparation of nitrogen-doped and surface-passivated carbon quantum dots with high quantum yield and excellent optical properties[J]. RSC Advances, 2014, 4(15): 7648-7654.
[27] Qu D, Zheng M, Du P, et al. Highly luminescent S, N co-doped graphene quantum dots with broad visible absorption bands for visible light photocatalysts[J]. Nanoscale, 2013, 5 (24): 12272-12277.
[28] Kundu S, Yadav R M, Narayanan T N, et al. Synthesis of N, F and S co-doped graphene quantum dots[J]. Nanoscale, 2015, 7(27): 11515-11519.
[29] Zhu C, Zhai J, Dong S. Bifunctional fluorescent carbon nanodots: green synthesis via soy milk and application as metal-free electrocatalysts for oxygen reduction[J]. Chemical Communications, 2012, 48(75): 936-9369.
[30] Wei J, Liu B, Yin P. Dual functional carbonaceous nanodots exist in a cup of tea[J]. RSC Advances, 2014, 4(108): 63414-63419.
[31] Liu Y, Liu C-Y, . Zhang Z-Y. Synthesis and surface photochemistry of graphitized carbon quantum dots[J]. Journal of Colloid and Interface Science, 2011, 356(2): 416-421.
[32] Dong Y, Pang H, Yang H B, et al. Carbon-based dots Co-doped with nitrogen and sulfur for high quantum yield and excitation-independent emission[J]. Angewandte Chemie International Edition, 2013, 52(30): 7800-7804.
[33] Bao L, Liu C, Zhang Z L, et al. Photoluminescence-tunable carbon nanodots: Surface-state energy-gap tuning[J]. Advanced Materials, 2015, 27(10): 1663-1667.
[34] Li H, Kang Z, Liu Y, et al. Carbon nanodots: synthesis, properties and applications[J]. Journal of Materials Chemistry, 2012, 22(46): 24230-24253.
[35] Li P, Huang L, Lin Y, et al. Printable temperature-responsive hybrid hydrogels with photoluminescent carbon nanodots[J]. Nanotechnology, 2014, 25(5): 055603-055608.
[36] Deng Z, Lie F L, Shen S, et al. Water-based route to ligand-selective synthesis of ZnSe and Cd-doped ZnSe quantum dots with tunable ultraviolet A to blue photoluminescence[J]. Langmuir, 2009, 25(1): 434-442.
[37] Sk M P, Jaiswal A, Paul A, et al. Presence of amorphous carbon nanoparticles in food caramels[J]. Scientific Reports, 2012, 2: 383.
[38] Aboulaich A, Geszke M, Balan L, et al. Water-based route to colloidal Mn-doped ZnSe and core/shell ZnSe/ZnS quantum dots[J]. Inorganic Chemistry, 2010, 49(23): 10940-10948.
[39] Costas-Mora I, Romero V, Lavilla I, et al. In situ building of a nanoprobe based on fluorescent carbon dots for methylmercury detection[J]. Analytical Chemistry, 2014, 86(9): 4536-4543.
[40] Zhu S, Meng Q, Wang L, et al. Highly photoluminescent carbon dots for multicolor patterning, sensors, and bioimaging [J]. Angewandte Chemie International Edition, 2013, 52 (14): 3953-3957.
[41] Zhang R, Chen W. Nitrogen-doped carbon quantum dots: Facile synthesis and application as a "turn-off" fluorescent probe for detection of Hg^{2+} ions[J]. Biosensors and Bioelectronics, 2014, 55: 83-90.
[42] Zhou L, Lin Y, Huang Z, et al. Carbon nanodots as fluorescence probes for rapid, sensitive, and label-free detection of Hg^{2+} and biothiols in complex matrices[J]. Chemical Communications, 2012, 48(8): 1147-1149.
[43] Chan Y H, Chen J, Liu Q, et al. Ultrasensitive copper(II) detection using plasmon-enhanced and photo-brightened luminescence of CdSe quantum dots[J]. Analytical Chemistry, 2010, 82(9): 3671-3678.
[44] Liang G, Liu H, Zhang J, et al. Ultrasensitive Cu^{2+} sensing by near-infrared-emitting CdSeTe alloyed quantum dots[J]. Talanta, 2010, 80(5): 2172-2176.
[45] Koneswaran M, Narayanaswamy R. L-Cysteine-capped ZnS quantum dots based fluorescence sensor for Cu^{2+} ion[J]. Sensors and Actuators B: Chemical, 2009, 139(1): 104-109.